SI Appendix
for

CAMSAP3 facilitates basal body polarity and the formation of the central pair of microtubules in motile cilia

Alan M. Robinson, Satoe Takahashi, Eva J. Brotslaw, Aisha Ahmad, Emma Ferrer, Daniele Procissi, Claus-Peter Richter, Mary Ann Cheatham, Brian J. Mitchell, Jing Zheng

Corresponding author: Jing Zheng
Email: jzh215@northwestern.edu

This PDF file includes:

- Supplementary text
- Tables SI to SII
- Figs. S1 to S16
- Captions for movies S1 to S9
- Captions for Audio S1
- References for SI Appendix reference citations

www.pnas.org/cgi/doi/10.1073/pnas.1907335117

Supplementary Information Text

Materials and Methods

Animals

All experimental procedures involving animals were conducted in accordance with the Guide for the Care and Use of Laboratory Animals by NIH and were approved by Northwestern University's Institutional Animal Care and Use Committee. *Camsap3*$^{tm1a\ (EUCOMM)\ Wtsi}$ *(referred to as Camsap3*^{tm1a} *in this study)* mouse model was purchased from the Wellcome Trust Sanger Institute. The *Camsap3*^{tm1a} mice were designed to ablate gene function by insertion of RNA processing signals without deletion of any exons of *Camsap3*. As shown in Fig. 1A, the inserted cassette includes a splice acceptor site from engrailed-2 (En-2 SA), and the internal ribosomal entry site (IRES) from the encephalomyocarditis virus (EMCV), and the SV40 polyadenylation signal (pA). Theoretically, CAMSAP3 proteins are not supposed to be made because *Camsap3* mRNA is truncated after exon 6. The original *Camsap3*^{tm1a} line on the C57B6N background was re-derived on FVB and CBA/CaJ murine backgrounds to increase their viability. Although we obtained viable *Camsap3*$^{tm1a/tm1a}$ mice on CBA/CaJ background, we failed to maintain this line due to their low reproduction rates. Most of the data were collected from FVB mice ranging from the F2 to the F7 generation unless specifically stated otherwise. All animals were maintained by heterotypic breeding, and genotypes were determined by Transnetyx (Cordova, TN). Both males and females were used in all experiments. Fertility rate was measured by pairing mice and monitoring the cages for births. *Camsap3*$^{tm1a/tm1a}$ was tested for both sexes by pairing *Camsap3*$^{tm1a/tm1a}$ with WT of the opposite sex. Homotypic breeding pairs for WTs were included as controls. For each breeding cage, expected numbers of litters were calculated by dividing the number of days in the breeding cage by 21. Average age of WT females having their first litter when paired with WT littermate males was determined to be at postnatal day 64. To obtain % fertility, observed numbers of litters for each cage were divided by expected litter numbers.

Xenopus *(embryo injection, plasmids, mRNA, and MOs)*

Xenopus embryos at the two- to four-cell stage were injected with mRNAs and MOs using standard protocols approved by the Northwestern University Institutional Animal Care and Use Committee (1). To synthesize mRNA, PCS2+ plasmids encoding Membrane-RFP, CLAMP-GFP, and Centrin4-RFP were linearized with Not1 and mRNA was generated by *in vitro* transcription using SP6 RNA polymerase (2). Morpholinos (Gene Tools, LLC) were used to target *Camsap3* (5'-GGCTTTAATCACAGGCACCATCATG-3') or a standard control (5'-CCTCTTACCTCAGTTACAATTTA TA-3').

Antibodies

A 96-aa peptide corresponding to amino acids of mouse CAMSAP3 (NM_001163749.1) at position 399-491 (SI Fig. S1A) was used to immunize rabbits and to generate an affinity-purified anti-CAMSAP3-M antibody (SDIX, Newark, Delaware). Sequence of the peptide is: RPLSQAVSFSTPFGLDSDVDVVMGDPVLLRSVSSDSLGPPRPVSTSSRNSAQPAPESGDLPTIEEALQI IHSAEPRLLPDGAADGSFLHSPEGLS. Information about other antibodies is listed in *SI Appendix* Table SII.

Evaluation of Olfaction

Mice were food restricted but provided water *ad libitum* for 16 hours prior to testing. Testing was performed during daylight, starting at 9 am. A Sterilite translucent storage box (cage) (47 cm (L) x 37.8 cm (W) x 28.3 cm (H)) was lined with paper and the base covered to a depth of 1.5 cm with bedding. The paper lining and the bedding were white for dark colored mouse tests and black for white mouse tests. A digital camera was placed 1 m above the cage and connected to a computer. Mice were placed individually in the cage without food and images captured over 5 minutes at a rate of 1 frame per second. Mice were then transferred individually to an identical cage, except that 0.5 g of bacon bits (Retail Human

food) were hidden in the center of the cage under the bedding and again images were captured over 5 minutes. Videos of mice in both cages were examined using custom Python software that determines how long the mouse was within the center of the cage. A visual identification of eating behavior was made to validate the method.

Measurements of Ciliary Motion

Euthanized animals were dissected to isolate either nasal tissue, the auditory bulla, or trachea. For nasal tissue isolation, coronal (frontal) sections were made with a double edge, thin razor blade, such that the primarily respiratory epithelium covering the anterior septum was represented, along with the motile cilia covering the anterior turbinates. Sections were ~1 mm thick. To isolate the ciliated respiratory regions of the auditory bulla, the tympanic ring was excised with Vannas type curved microscissors. Ventral neck tissues were removed to visualize the trachea, which was excised to cut ~1 mm tracheal rings. The medial wall of the bulla was cut open and the bulla cut in half to create two cup-like anterior and posterior halves. The posterior half had a region of ciliated epithelium, that when *in situ*, is located superior and medial in the bulla and close to the cochlea. This region was not used for cilia analysis because the area is not extensive and ciliated cells tend to be relatively sparse. The anterior part of the bulla contained the cut edge of the bulla lateral to the entrance to the Eustachian tube. This edge was used to microscopically visualize cilia. The extensive, ciliated epithelium in this area is "carpet-like," as found in the nasal respiratory epithelium, and extends into the Eustachian tube. Tissues were briefly immersed in lactate buffered Ringer's solution (Alfa Aesar, MA) to remove excess mucus and blood. For all tissues, a small amount of petroleum jelly (Vaseline) was placed just off center onto the surface of an optically clear plastic macrowell culture plate using a cotton-tipped swab. The tissue sample was then placed on the well culture surface close to the petroleum jelly. Forceps were used to drag some petroleum jelly to the edge of the tissue to anchor it. Care was taken to avoid touching any areas where cilia would be located, such that the jelly only contacted the bony exterior surface of the tissue. 3 ml of lactate-buffered Ringer's solution (Alfa Aesar, MA) was carefully added to the well to avoid dislodging the tissue. Assay buffer temperature was measured using a non-contact laser thermometer and was consistently 25 ± 0.6 ºC. Cilia were oriented such that they were approximately perpendicular to the transmitted light of a Leica DMLB microscope. The microscope condenser was adjusted to an offset position to create a shadow to improve cilia visualization. A standard 5x air lens was used to guide coarse tissue positioning, and the cilia were then observed using a 63x water-dipping lens. An Edmund Optics USB3 high-speed camera was mounted onto the microscope and linked to a 64 bit PC with an AMD FX(tm) 6300 six core 3.5 GHz processer with 32 GB RAM, running Windows 10. The camera was controlled by Eye Cockpit software (IDS, Obersulm, Germany). Video sequences of cilia motion, at least 512 frames in length, were captured at frame rates around 600 frames per second (fps) by cropping the field of view to a region of interest encompassing the motile cilia. Videos with 100% successful frame transfer to the computer hard drive were used for subsequent data analysis.

The open source software CiliaFA plugin for imageJ (3) was used to analyze digital video files (.avi format) of cilia motion. The analysis was performed as described previously (4) and has been validated by the authors to give accurate cilia beat frequency (CBF) data using a minimum of 128 video frames taken at 120 frames per second to give a 0.94 Hz frequency resolution. In brief, the software divides the frame into a 40 x 40 grid and measures the pixel intensity at each cell over time. The data set is automatically exported to a Microsoft Excel spreadsheet (specific for respiratory cilia beat frequencies of 3-20 Hz) and a visual basic macro routine performs a Fast Fourier Transform (FFT) on the data set. The mean median and modal cilia beat frequencies were reported and cilia beat frequencies of < 3 Hz were reported as 0 Hz.

For imaging fluid flow on Xenopus embryos, control or Camsap3 MO-injected embryos were placed in a dish with a V-shaped barrier. 10 µm fluorescent microspheres (FluoSpheres, Thermo Fisher, F8836) were then applied on the surface of embryos and imaged using Leica M165 FC Fluorescence Stereomicroscope (Leica) controlled by LAS Core (Leica) at the frame rate of 1 Hz. Mean distance of each fluorescence bead traveled per second was determined by averaging the distance for three consecutive frames, and then grouped for experimental conditions.

Measurement of Cilia Orientation

To measure the cilia orientation of Camsap3 morphant or control morphant embryos, embryos were injected with CLAMP-GFP and Centrin4-RFP to mark the rootlets and basal bodies, respectively. Embryos were grown until stage 26-28 and fixed in 3% paraformaldehyde in PBS. Embryos were imaged with a Nikon A1R confocal microscope using a 60X Plan/Apo, 1.4 NA oil objective lens, and then manually scored for rootlet orientation using ImageJ. Oriana2 was used for all circular statistics and graphing (1).

Audio Recording and Analysis

Aged-matched WT and *Camsap3*$^{tm1a/tm1a}$ mice were placed into a shoebox-sized cage in a sound-attenuating chamber. A Knowles surface mount MEMS microphone was placed together with its preamplifier into the cage on one of the short sides. Animal wheezing was recorded at a sampling rate of 250 kHz using a KPCI-3110 computer analog-to-digital PCI board (Keithley). The traces were analyzed subjectively by listening to the resulting sounds. Since the signals varied over time, short time Fourier transformations (STFT) were used to analyze the recordings. The plots shown in *SI Appendix* Fig. S4 were calculated with a window size of 1024 points, a frame shift of 1 point and 1024 points for the STFT. The resulting spectrograms show on the x-axis the time of the recording and along the y-axis the frequencies. Since frequencies above 20 kHz are inaudible to humans, the same sound track was played at a fifth of the original sampling rate.

Histochemistry

Following euthanasia with Euthasol (200 mg/Kg, IP) or CO_2 plus thoracotomy, mouse pups were fixed without perfusion with 4% paraformaldehyde in phosphate buffered saline (PBS, pH 7.4) and adult mice were fixed by cardiac perfusion with PBS pH 7.4 followed by 4% paraformaldehyde in PBS. Heads were then post-fixed in the same fixative overnight at 4˚C. Three washes of PBS were performed and heads decalcified for a week in 10% EDTA pH 7.0 at 4˚C. Heads were washed three times in PBS pH 7.4 and passed through 20 min baths of 50%, 70%, 80% and 95% ethanol in water followed by two more changes of 95% ethanol and three changes of 100% ethanol, followed by 3 changes of 10 minutes each of xylene until tissue cleared. A 50% xylene, 50% molten Paraplast-Xtra (Sigma-Aldrich, St. Louis, MO) wax bath was applied for 20 minutes followed by three changes of 100% wax for infiltration. Fresh wax was then used for the final embedding using a metal mold. Tissue blocks were sectioned on a rotary microtome at 5-10 µm and sections adhered to glass microscope slides overnight at 56˚C. Tissues were dewaxed in three 5 min changes of xylene followed by three changes of 100% ethanol and two changes of 95% ethanol, each for 1 min and then two changes of distilled water to rehydrate the tissue. Tissues were then subjected to either Periodic Acid Schiff (PAS) or Hematoxylin & Eosin (H&E) staining. The PAS stain demonstrates glycoproteins such as those in mucins as shades of pink to magenta, while the H&E stain shows many structures and is a common pathology stain to identify cellular structures. The PAS stain was as per the manufacturer's (American MasterTech, Lodi, CA., P.A.S. satin kit cat# KTPAS) instructions. In brief, a 5 min oxidation in 0.5% periodic acid, water rinse, followed by 15 min color development in Schiff reagent, 1 min counterstain in Mayer hematoxylin and fast green, ending with a tap water rinse (5). For H&E staining, tissue sections were incubated in Harris's hematoxylin for 5 min, tap water wash 5 min, 30 s in 1% HCl, tap water 1 min, 1 min in 0.2% ammonia water, tap water 5 min, 10 dips in 95% ethanol, 30 s in 1% Eosin with 0.1% Phloxine B in 95% ethanol, 4% glacial acetic acid (6). For both PAS and H&E stains dehydration was accomplished with two changes of 95% ethanol and three changes of 100% ethanol, 5 minutes each followed by dehydration in two changes of xylene, 5 min each followed by cover glass mounting with Permount (Electron Microscopy Sciences, Hatfield, PA). For OMP immunohistochemistry, non-specific antibody binding was blocked by a 5% v/v goat serum in pH 7.4 PBS incubation for 30 min at room temperature in a humidified chamber. Next, sections were incubated at room temperature with 1:2000 goat anti-OMP. Sections were washed in pH 7.4 PBS and incubated with biotinylated ant-goat IgG for 30 min followed by a PBS wash for 5 min. Sections were then incubated for 30 min with avidin with biotinylated horseradish peroxidase (a rabbit anti-goat Vectastain Elite ABC kit) and washed with PBS again. A brown color was generated by incubation with diaminobenzidine (DAB) peroxidase substrate to localize OMP protein. Sections were counterstained

with hematoxylin, dehydrated through graded ethanol baths, then xylene and coverslips applied with Permount. A similar protocol was followed for CAMSAP3 immunohistochemistry, except that the antibody used was rabbit anti-CAMSAP3-M antibody (188 ng/ml), the Vectastain Elite ABC kit was Rabbit IgG, and the peroxidase substrate was Vector NovaRED.

Transmission Electron Microscopy (TEM)

Nasal septae and turbinates from WT and *Camsap3*$^{tm1a/tm1a}$ mice were fixed in 0.1 M sodium cacodylate buffer pH 7.3, containing 2% paraformaldehyde and 2.5% glutaraldehyde for at least 24 hours and post-fixed with 2% osmium tetroxide then 3% uranyl acetate. Tissues were dehydrated in ascending grades of ethanol, transitioned with propylene oxide and embedded in resin mixture of Embed 812 kit, cured in a 60˚C oven. Samples were sectioned on a UCT ultramicrotome (Leica Microsystems). To identify regions of interest 1 µm thick sections were collected, stained with Toluidine Blue O and examined by light microscopy. 70 nm tissue sections were collected on 200 mesh copper grids and stained with uranyl acetate and Reynolds lead citrate, and examined using a FEI Tecnai Spirit G2 Transmission Electron Microscope.

Scanning Electron Microscopy (SEM)

Nasal septae and turbinates from WT and *Camsap3*$^{tm1a/tm1a}$ mice were dissected and then fixed in 2.5% glutaraldehyde in 0.1 M PBS (pH 7.4) overnight at 4°C and a post-fixed in 1% OsO4 in 0.1 M PBS (pH 7.4) for 1 hour. Samples were washed in 0.1 M PBS (pH 7.4), followed by sequential dehydration with 20%, 40%, 60%, 80%, 95%, and 3×100% ethanol for 10 min each. Dehydrated samples were sputter-coated with gold using the Baltec coating system and imaged on the JEOL Neo Scope Benchtop SEM.

Micro-computed Tomography (micro-CT) and Magnetic Resonance Imaging (MRI)

Micro-CT was conducted on anesthetized mice (isofluorane + 100% O_2) using a nanoScan8 PETCT system (Mediso, Budapest, HU). The 3D images were obtained from 740 projections acquired at 75 KeV with exposure time of 150 msec for each projection. The final resolution was 60 microns isotropic. MRI was conducted on anesthetized mice (isofluorane + 100% O_2) using a Bruker CLinscan 7T. MR 3D images at 150 micron resolution were acquired using a gradient echo sequence with TR=100 msec and TE=3 msec. A dedicated 4 channel receive-only surface coil was placed on the mouse head and centered over the nasal region to optimize signal reception with a quadrature volume coil used for transmission. During CT and MRI scans the animals were maintained at physiological temperature using built in heating units and respiration was monitored throughout the experiments.

Immunofluorescence Microscopy

Neonatal samples of cochleae, nasal septae, and turbinates from WT and *Camsap3*^{tm1a} mice were fixed with 2% formaldehyde/PBS for 1 hour at room temperature. Adult mice were first cardiac perfused with PBS and then with 2% formaldehyde/PBS for 1 hour at room temperature for fixation. Adult samples were decalcified in 10% EDTA/PBS at 4°C 1-2 days. Decalcified samples were placed in a series of sucrose solutions in 1X PBS (10%-30%) then two changes of OCT and embedded in fresh OCT. Nasal samples were cut into 5-10 micron sections, placed on glass slides, fixed in 2% formaldehyde for 10 minutes and blocked at room temperature for 1 hour in blocking solution: 5% goat serum, 2% Triton X-100 in 1X TBS (Tris-buffered saline). Samples were then incubated with anti-CAMSAP3-M (56.5 ng-282 ng/ml), anti-acetylated-α-tubulin (1:500), anti-γ-tubulin (1:200) at 4 °C overnight, followed by incubation with goat anti-rabbit-IgG (1:500) and anti-mouse IgG2b (1:1000) or anti-mouse IgG1 (1:500) conjugated with AlexaFluor-488, AlexaFluor-568, and AlexaFluor-647. Hoechst 33342 was also included to stain nuclei (7). Stained sections were mounted using Fluoromount Aqueous Mounting Medium (Sigma) for imaging. To visualize cilia on MCCs of Xenopus embryo skin, a previously described protocol was used (1). Briefly, fertilized Xenopus eggs at 2-4 cell stage were injected with control or Camsap3 morpholinos (Gene Tools, LLC) with membrane marker (mem-RFP), developed until stage 24-28, fixed in 3%PFA in PBS for 2 hours at room temperature. Anti-acetylated-α-tubulin followed by Cy2-conjugated anti-mouse antibodies for cilia, and Cy-7 conjugated phalloidin for actin were used. Images were captured using A1R+ confocal

microscope (Nikon) and N-SIM Structured Illumination Super-resolution Microscope (Nikon), and analyzed using Image J and Nikon NIS Element software.

RT-PCR Analysis of Camsap3 Transcripts

After animals were euthanized with an overdose of anesthetic (Euthasol 200 mg/kg), cochlear samples from WT and *Camsap3*$^{tm1a/tm1a}$ mice were dissected and immediately put into lysis buffer and processed using the Absolutely RNA Miniprep Kit (Agilent). cDNA synthesis was carried out with 0.5 µg of total RNA and random primers using M-MLV-RT (Promega). PCR reactions were performed using GoTaq Flexi DNA polymerase and 2 µl of cDNA and a specific primer set annealing to downstream of *Camsap3* Exon 7 (Kiaa A RT 2: 3'- GGCACAACTGAAACTGATGG -5'; Kiaa B RT 2: 3'- CATTGCTTCCATTCTCCCAG -5') and a house keeping gene *Cyclophilin*: (CycloA: 3'-TGGCACAGGAGGAAAGAGCATC-5'; CycloB: 3'- AAAGGGCTTCTCCACCTCGATC -5') (8). The following PCR program was used: initial denaturation, 95 ºC 2 min; 35 cycles 95 ºC 30 sec, 55 ºC 45 sec, 72 ºC 30 sec; final extension at 72 ºC, 5 min. PCR products were analyzed on 1.5% agarose gel with 100bp ladder (Thermo 15628-019).

Protein Analysis using Western Blotting

Brain tissues were dissected from *Camsap3*^{tm1a} WT, *Camsap3*$^{tm1a/+}$, and *Camsap3*$^{tm1a/tm1a}$ mice at P10-11. Tissues from the same litter were lysed in RIPA buffer (10 mM Tris-Cl pH 8, 1 mM EDTA, 0.5 mM EGTA, 1% TritonX-100, 0.1% SDS, 140 mM NaCl) supplemented with 1X protease inhibitor cocktail (Sigma), 1 mM PMSF, and 10 µg/ml DNase I. Protein concentrations in the lysates were measured using the Thermo 660 nm protein assay reagent. 50 µg of total lysates were loaded per lane of a 4-20% gradient gel, transferred to nitrocellulose membrane with CAPS buffer (pH 11), and CAMSAP3 detected by anti-CAMSAP3-M (22.6-113 ng/ml), followed by goat anti-rabbit IgG-HRP (1:5000). For the loading control, Tubulin was detected by anti-α-Tubulin (1:2000) and goat anti-mouse HPR (1:5000). Signals were detected using Amersham ECL Prime Western Blotting Detection Reagent (GE). A Kodak Imaging System was used to capture the images. Band intensities of CAMSAP3 and Tubulin were measured using ImageJ and plotted using Prism 7 (GraphPad).

Cell Culture and Transfection

Plasmids encoding V5 or GFP tagged mouse *Camsap3* (9) and GFP-tagged human CAMSAP2 (obtained from Anna Akhmanova) (10) were transiently transfected into OK (opossum kidney) and HEK293 cells as previously described (9). 24-45 hours post transfection, cells were collected and lysed for Western blot or were fixed with 2% formaldehyde for immunofluorescence (IF). For immunofluorescent experiments, cells were incubated with monoclonal anti-V5 and rabbit polyclonal anti-CMSAP3-M for 1 hour, followed by incubation with secondary antibodies, goat anti-mouse IgG-Alexa Fluor 546 and goat anti-rabbit IgG-Alexa Fluor 488. Samples were imaged using A1R+ confocal microscope (Nikon). In SDS/PAGE Western blot experiments, cells were lysed in cold lysis buffer (50 mM Tris-HCl, pH 7.6, 150 mM NaCl, 1% Triton X-100) supplemented with a protease inhibitor cocktail (1:100) and 100 µg/ml PMSF. Insoluble material was removed by centrifugation at 10,000 xg for 15 minutes. Proteins were resolved using 4-20% SDS-PAGE, transferred to nitrocellulose membrane with CAPS buffer (pH 11), followed by immunoblotting using anti-CAMSAP3-M, anti-GFP, or anti-α-tubulin followed by anti-rabbit IgG-HRP or anti-mouse IgG-HRP. Signals were detected using SuperSignal West Pico Chemiluminescent Substrate (Thermo). A Kodak Imaging System was used to capture the images.

Statistical Analyses

Any changes in anatomy, protein quantity, and/or physiology were statistically analyzed (Chi-square test, ANOVA, t-tests, Tukey-Kramer test, Dunnett's multiple comparison test, circular statistics) to determine significance as described before (7, 11, 12). Values of $p < 0.05$ were considered to indicate statistical significance.

TABLES

Table SI. Mendelian inheritance in the offspring of *Camsap3*^{tm1a} mice lines

Strain	Genotype	Total #	% Observed (%Expected)	Significance
C57B6N	WT	41	39.42 (25)	χ^2=32.37
	Camsap3$^{tm1a/+}$	61	58.65 (50)	p<0.0001
	Camsap3$^{tm1a/tm1a}$	2	1.92 (25)	Yes
CBA/CaJ	WT	13	35.14 (25)	χ^2=2.676
	Camsap3$^{tm1a/+}$	18	48.65 (50)	p = 0.2624
	Camsap3$^{tm1a/tm1a}$	6	16.22 (25)	No
FVB	WT	45	22.17 (25)	χ^2=1.266
	Camsap3$^{tm1a/+}$	109	53.69 (50)	p = 0.5310
	Camsap3$^{tm1a/tm1a}$	49	24.14 (25)	No

Table SII. Antibodies and Chemicals

Antibodies	**SOURCE**	**IDENTIFIER**
Rabbit anti-CAMSAP3-M	Zheng Lab	
Rabbit anti-CAMSAP2	Proteintech 17780-1-AP	RRID: AB_2068826
Mouse anti-α-tubulin	Sigma T6199	RRID: AB_477583
Mouse anti-acetylated-α-tubulin (IgG2b)	Thermo Fisher 32-2700	RRID: AB_2533073
Mouse anti-V5	Thermo Fisher R960-25	RRID: AB_2556564
Mouse anti-γ-tubulin (IgG1)	Santa Cruz sc-51715	RRID: AB_630410
Mouse anti-GFP (Living Colors® A. v. monoclonal antibody, JL-8)	Takara Bio USA 632380	RRID AB_10013427
Goat anti-OMP	FUJIFILM Wako-Chemicals U.S.A. Corp.	
Goat anti-rabbit Alexa 488 conjugated	Thermo Fisher	RRID: AB_143165
Goat anti-mouse IgG1 Alexa 568 conjugated	Thermo Fisher	RRID: AB_141611
Goat anti-mouse IgG2b Alexa 647 conjugated	Thermo Fisher	RRID: AB_1500900
Peroxidase-AffiniPure goat anti-mouse IgG (H+L)	Jackson ImmunoResearch Lab 115-035-146	RRID: AB_2307392
Goat anti-rabbit IgG-HPR conjugated	Thermo Fisher 14-9965-80	RRID: AB_1548836
Dylite 650 conjugated phalloidin	Thermo Fisher 21838	RRID: AB_2532159
Cy2-AffiniPure Donkey anti-mouse antibodies IgG (H+L)	Jackson ImmunoResearch Lab 715-225-150	RRID: AB_2340826
Rabbit anti-goat Vectastain Elite ABC kit	Vector Laboratories, Inc., Burlingame, CA	PK-6101 LOT ZF0607
Chemicals		
Hoechst 33342	Thermo, H3570	
NovaRED Substrate kit, Peroxidase	Vector Laboratories, Inc., Burlingame, CA	SK-4800 LOT ZF0710
DAB Substrate kit, Peroxidase	Vector Laboratories, Inc., Burlingame, CA	SK-4105

FIGURES

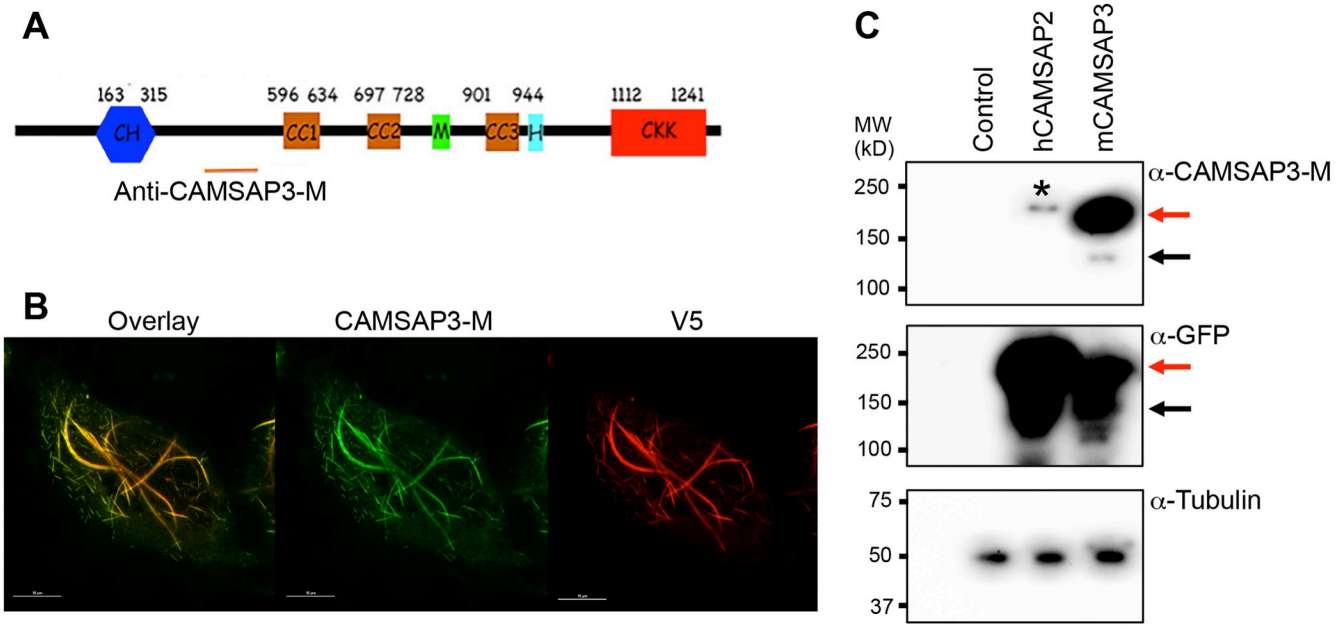

SI Figure S1. Specificity validation of the anti-CAMSAP3-M antibody. **A**. The structure of CAMSAP3. The orange line indicates the antigen location for anti-CAMSAP3-M. Protein-Protein interaction domains: CH, calponin homology; CC, coiled coil; M, microtubule-binding domain; H, helical domain; CKK, carboxy-terminal tubulin-binding domain. **B**. Validation of anti-CAMSAP3-M immunofluorescence. Opossum kidney (OK) cells were transfected with plasmids encoding mouse CAMSAP3-V5-His. The expression of CAMSAP3 with C-terminal V5-His tags in OK cells was detected by anti-CAMSAP3-M (middle, green) and anti-V5 (left, red) antibodies. The left image superimposes green and red images to indicate that the staining for V5 and CAMSAP3 overlaps. Similar staining patterns for both antibodies indicate that anti-CAMSAP3-M recognizes CAMSAP3 protein (n=6). Scale bars, 10 μm. **C**. Validation of anti-CAMSAP3-M in Western blot. HEK293T cells transfected with control, human CAMSAP2-GFP, and mouse CAMSAP3-GFP constructs were collected for Western blot analysis. Livingcolors JL-8 (GFP) antibody was used to detect GFP that was attached to the C-terminus of CAMSAP2 and CAMSAP3 proteins, and anti-α-tubulin was used to detect tubulin, the loading control. Expression of CAMSAP3-GFP was detected by both anti-GFP and anti-CAMSAP3-M antibody (56.5 ng/ml). The same molecular weight bands were recognized by both anti-GFP and anti-CAMSAP3-M: the full-length CAMSAP3-GFP protein (red arrow) and a smaller band (back arrow). The small band is likely a degraded fragment from CAMSAP3-GFP as the same size band was also recognized by anti-GFP. In addition, a faint band in the hCAMSAP2-GFP lane was also detected by anti-CAMSAP3 (*). Judging from the intensities of signals detected by anti-GFP, a significant amount of hCAMSAP2-GFP was present in the sample. These data suggest that anti-CAMSAP3-M has much higher affinity for CAMSAP3 than for CAMSAP2 (n=3).

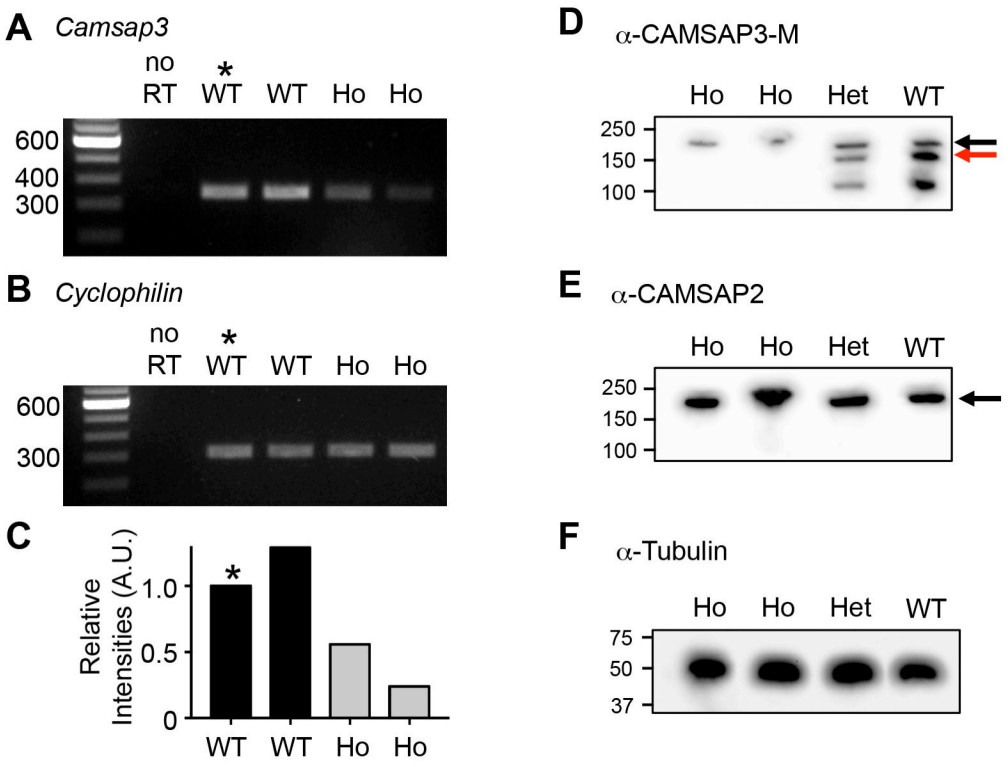

SI Figure S2. *Camsap3* expression is reduced, but not eliminated, in *Camsap3*$^{tm1a/tm1a}$. **A-C**. Semi-quantitative RT-PCR showing Camsap3 mRNA expression in cochleae of *Camsap3*$^{tm1a/tm1a}$ (Ho). The expected 338 bp products for *Camsap3* (**A**) and 301 bp for *Cyclophilin* (**B**) were observed in both WT and *Camsap3*$^{tm1a/tm1a}$ samples. Reaction without RT (no RT) was included as negative control. **C**. Quantitation showing the relative band intensities from reaction **A** normalized to that of **B**, and plotted using one of the WT samples (*) as the reference. *Camsap3*$^{tm1a/tm1a}$ showed reduced levels of *Camsap3* mRNA compared to WT. **D-E**. Representative images of Western blot showing expression of CAMSAP3 proteins in *Camsap3*^{tm1a} mice. Brain lysates from P10 WT, *Camsap3*$^{tm1a/+}$, and *Camsap3*$^{tm1a/tm1a}$ littermates were detected using anti-CAMSAP3-M (**D**), anti-CAMSAP2 (**E**), and anti-α-Tubulin (**F**) antibodies. Anti-CAMSAP3-M recognized two bands. The red arrow (**D**) indicates the expected band for CMASAP3, which is absent or reduced signal intensity in the lanes of *Camsap3*$^{tm1a/tm1a}$ samples. Because anti-CAMSAP3-M also recognized CAMSAP2 with much lower affinity (*SI Appendix* Fig. S1C), the **D** blot was stripped and re-probed with anti-CAMSAP2 (1:20,000). The upper band was recognized by anti-CAMSAP2 (**E**). Because CAMSAP2 is highly expressed in neurons/brain (13, 14), it is not surprising that anti-CAMSAP3-M detected CAMSAP2 signal in brain lysates. The bands lower than CAMSAP3 were likely fragments degraded from the full-length CAMSAP3 or potential isoforms (9) as they were not visible in lanes of *Camsap3*$^{tm1a/tm1a}$ samples. The signal intensities of CAMSAP3 (indicated by red arrow) and tubulin were measured, and tubulin was used as loading control. Quantitation from three independent experiments are shown in **Fig. 1B**.

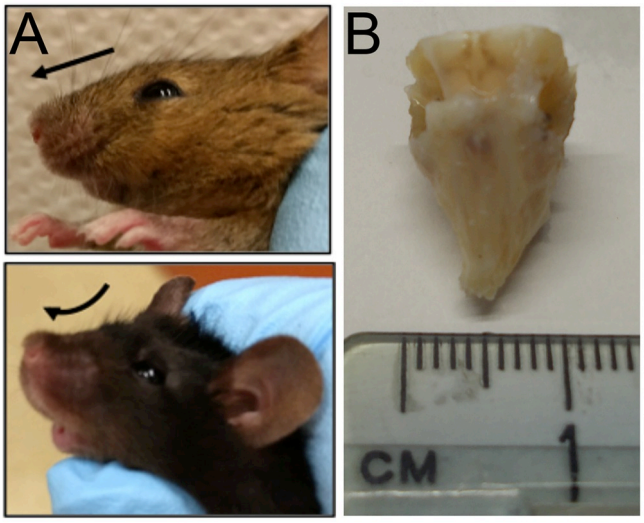

SI Figure S3. A. Abnormal upturned snout and domed head in an adult *Camsap3*$^{tm1a/tm1a}$ (Homo) in CBA/CaJ strain background (lower, P194) as compared to a WT littermate (Top). **B.** Snout asymmetry observed in a *Camsap3*$^{tm1a/tm1a}$ in CBA/CaJ strain background, showing deviation to the right.

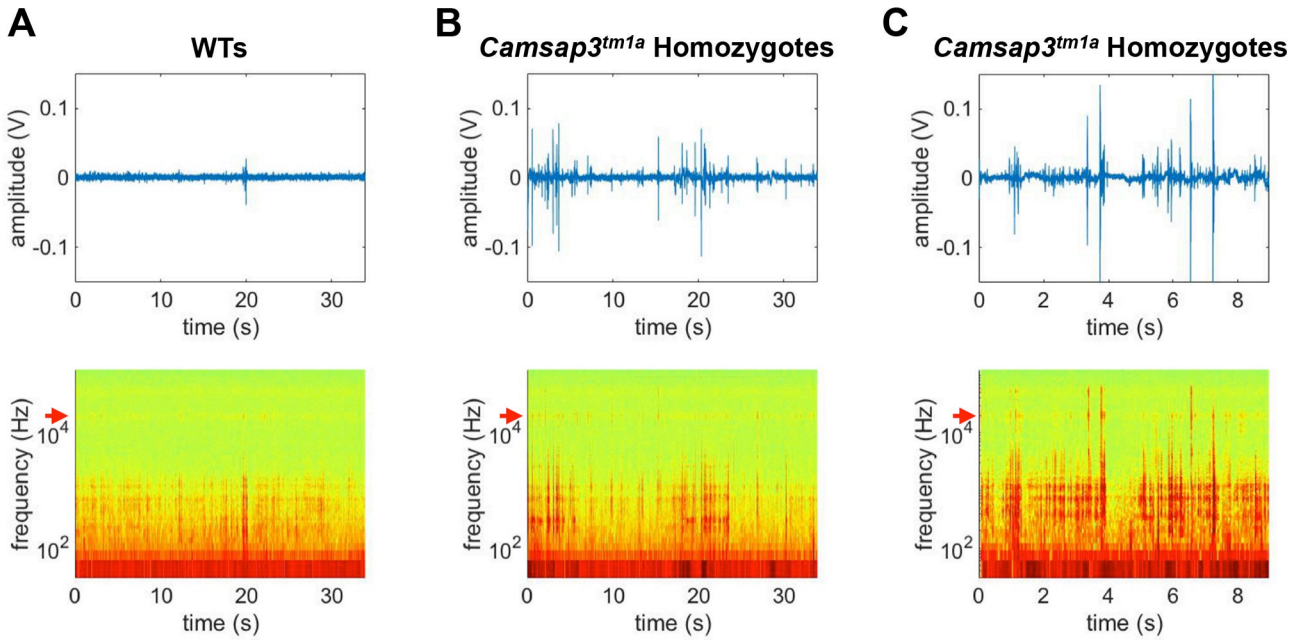

SI Figure S4. Audio recordings from WT and *Camsap3*$^{tm1a/tm1a}$ mice. **A**. A trace of microphone voltage (top) and a spectrogram (bottom) of the sound recordings from a group of WT mice. The frequency components above and below 20 kHz (arrow) are small. **B.** Microphone voltage (top) and the companion spectrogram (bottom) from a group of *Camsap3*$^{tm1a/tm1a}$ mice showing higher amplitudes and additional frequency components. The recordings in *Camsap3*$^{tm1a/tm1a}$ are much noisier than in controls. **C.** Another shorter recording (10 seconds) from the same group of *Camsap3*$^{tm1a/tm1a}$ mice. Multiple frequency components, including those above 20 kHz (**C**, arrow), are clearly shown. The corresponding sound file for (**C**) is provided in *SI Appendix* Audio S1.

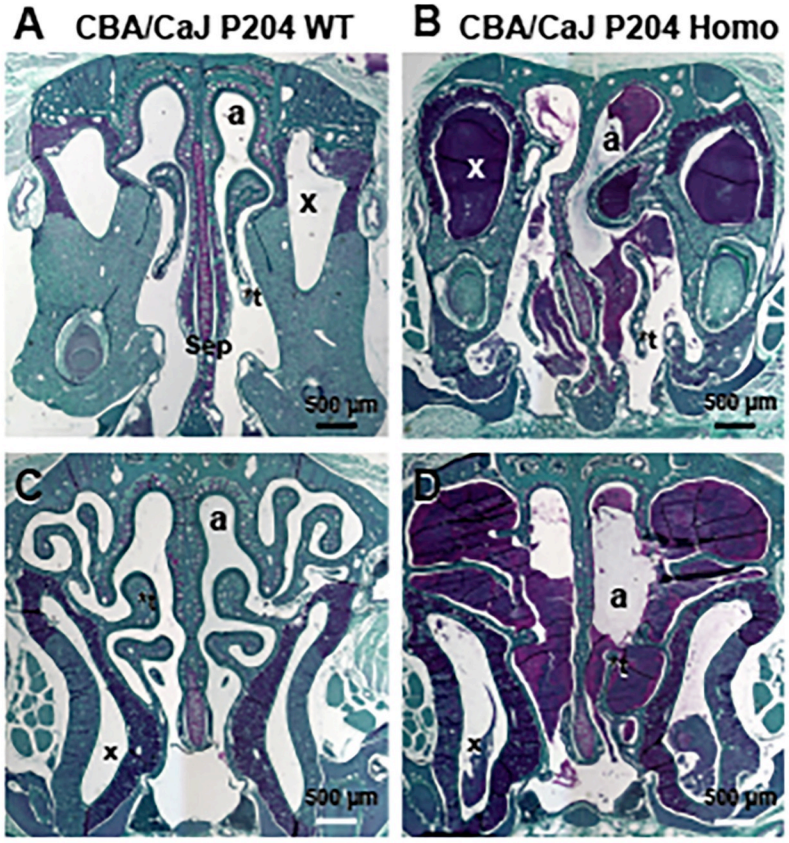

SI Figure S5. Older *Camsap3*$^{tm1a/tm1a}$ showing mucin accumulation in nasal cavity including sinus. WT (**A, C**) frontal section of P204 CBA/CaJ mouse head stained with PAS showing a patent maxillary sinus (x) and airway (a). The septum (Sep) is vertical and the turbinates are of normal appearance (*t), while the *Camsap3*$^{tm1a/tm1a}$ littermate (**B, D**) shows mucin secretions (m, stained magenta/purple) filling the maxillary sinus (x) and obstructing the airway (a). Scale bars, 500 μm.

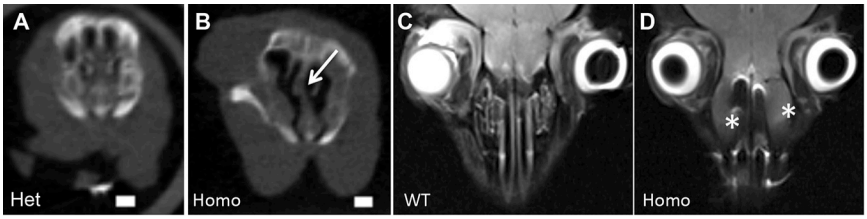

SI Figure S6. Airway blockage and structural abnormality in young adult *Camsap3*$^{tm1a/tm1a}$**.** Micro-CT (**A-B**) and MRI (**C-D**) images of young adult *Camsap3*$^{tm1a/+}$ (**A**), WT (**C**) and *Camsap3*$^{tm1a/tm1a}$ (**B, D**), showing deviated septum (**B**, arrow) and airway blockage (**D**, *) in the posterior nasal cavity. Scale bar, 2 mm.

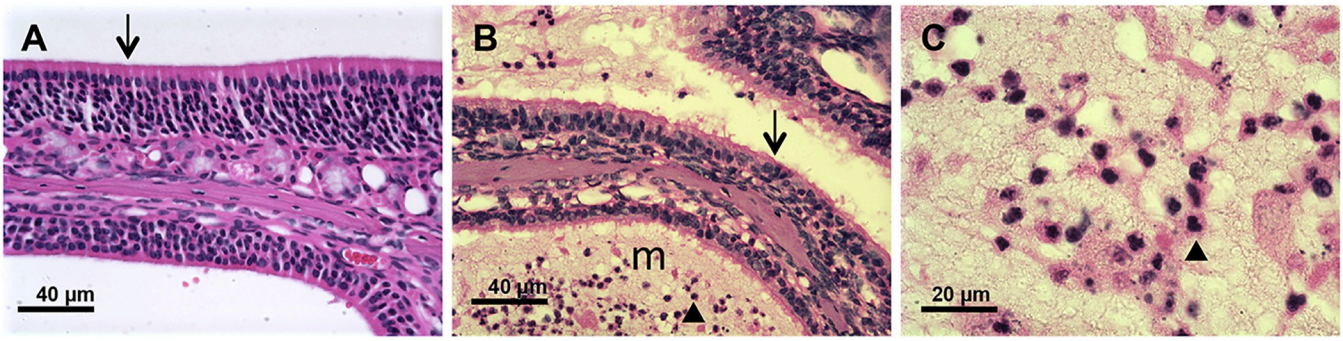

SI Figure S7. Infection in the nasal cavity of *Camsap3*$^{tm1a/tm1a}$ mice. High magnification of a non-infected WT (**A**) turbinate stained with H&E showing a thick olfactory epithelium on the superior surface (arrow). In contrast, the *Camsap3*$^{tm1a/tm1a}$ (**B**) shows a much thinner olfactory epithelium (arrow) bathed in a sea of mucus (m) with leukocyte infiltrate (blue arrowhead), which are shown at higher magnification in panel **C**. Scale bars: 40 µm (**A-B**), 20 µm (**C**).

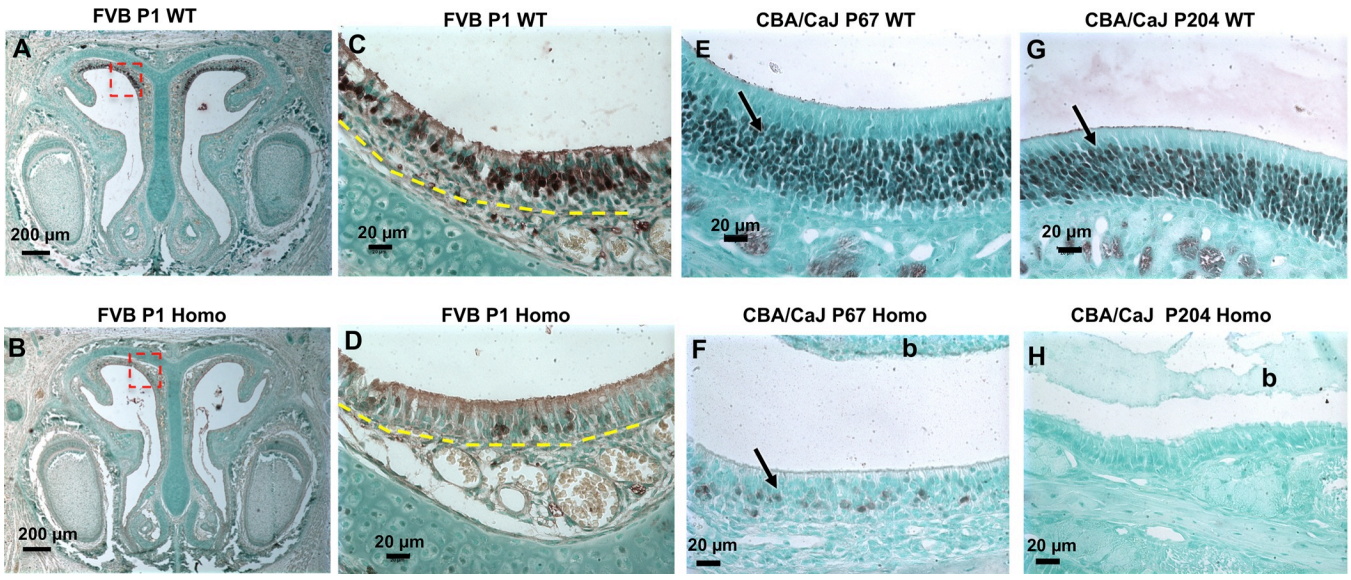

SI Figure S8. Anti-OMP staining showing OSN distribution at three ages: neonatal (P1, **A**-**D**), young adult (P67, **E**-**F**), and older adult mice (P204, **G**-**H**). **A**-**D**: Fewer mature OSNs (brown, NovaRED stain) in P1 *Camsap3*$^{tm1a/tm1a}$ (**B**, **D**) than WT (**A**, **C**). **C**-**D** are enlarged images of the boxed regions in **A**-**B**. The olfactory epithelium (OE) layer lies above the yellow line. **E**-**H**: Progressive nasal blockage and loss of OSNs in *Camsap3*$^{tm1a/tm1a}$ mice. A two-month-old WT (**E**) shows a thick layer of mature OSNs (arrow) compared to a thin epithelium populated with only a few mature OSNs (arrow) in an age-matched *Camsap3*$^{tm1a/tm1a}$ (**F**), which also exhibits mucus and debris build-up (b). At ~7 months (**G**), the typical mature olfactory epithelium is evident in WT (arrow), however, mature OSNs are largely absent in the epithelium of the age-matched *Camsap3*$^{tm1a/tm1a}$ (**H**) and the mucus and debris build-up is extensive (b).

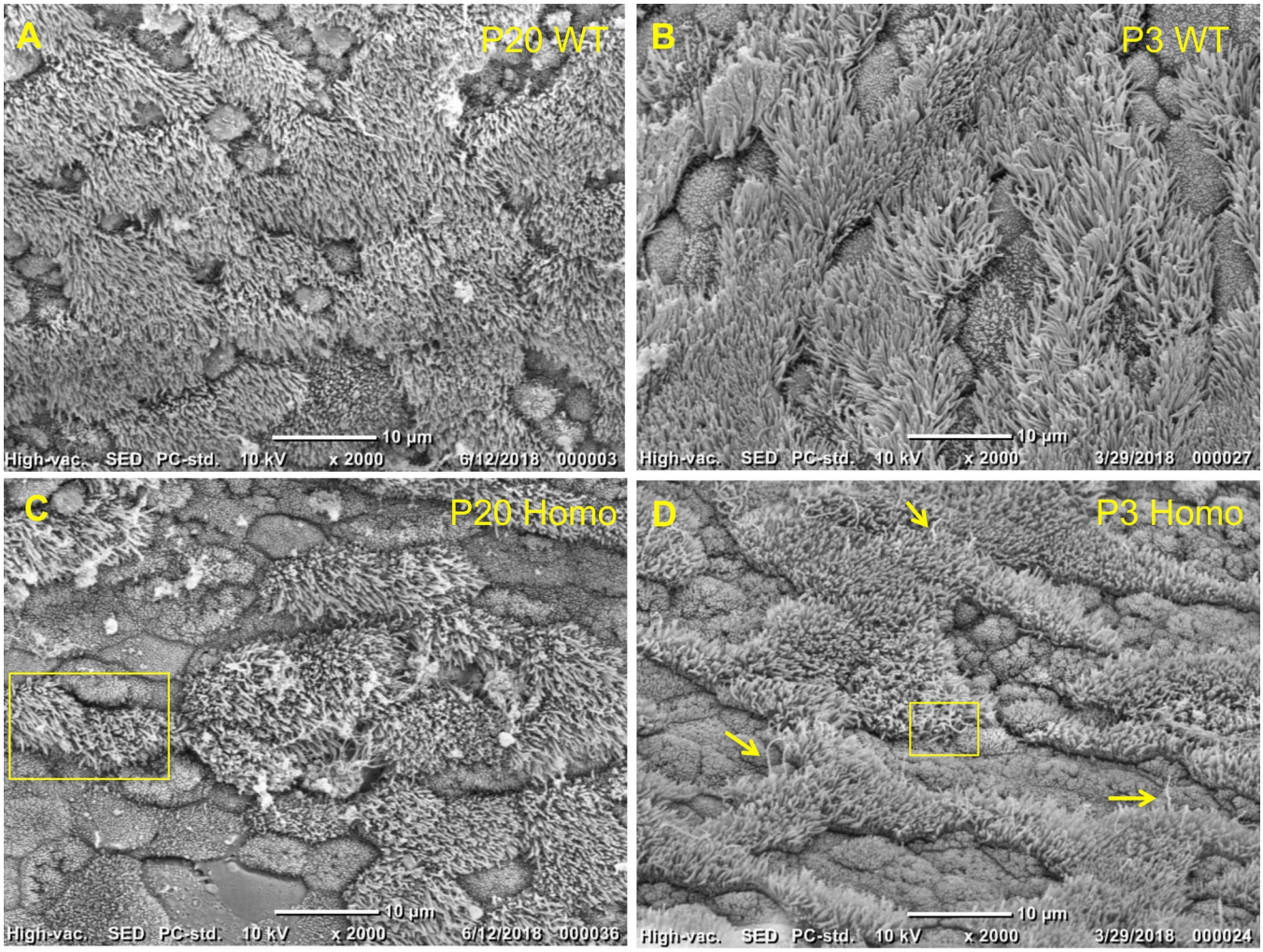

SI Figure S9. Scanning electron micrographs (SEM) of nasal respiratory epithlium. (**A**) P20 wild type (WT) compared to (**C**) P20 *Camsap3*$^{tm1a/tm1a}$. (**B**) P3 WT compared to (**D**) P3 *Camsap3*$^{tm1a/tm1a}$. Arrows show long cilia. Yellow boxes shown in higher magnification in Fig. 3. Bars = 10 µm.

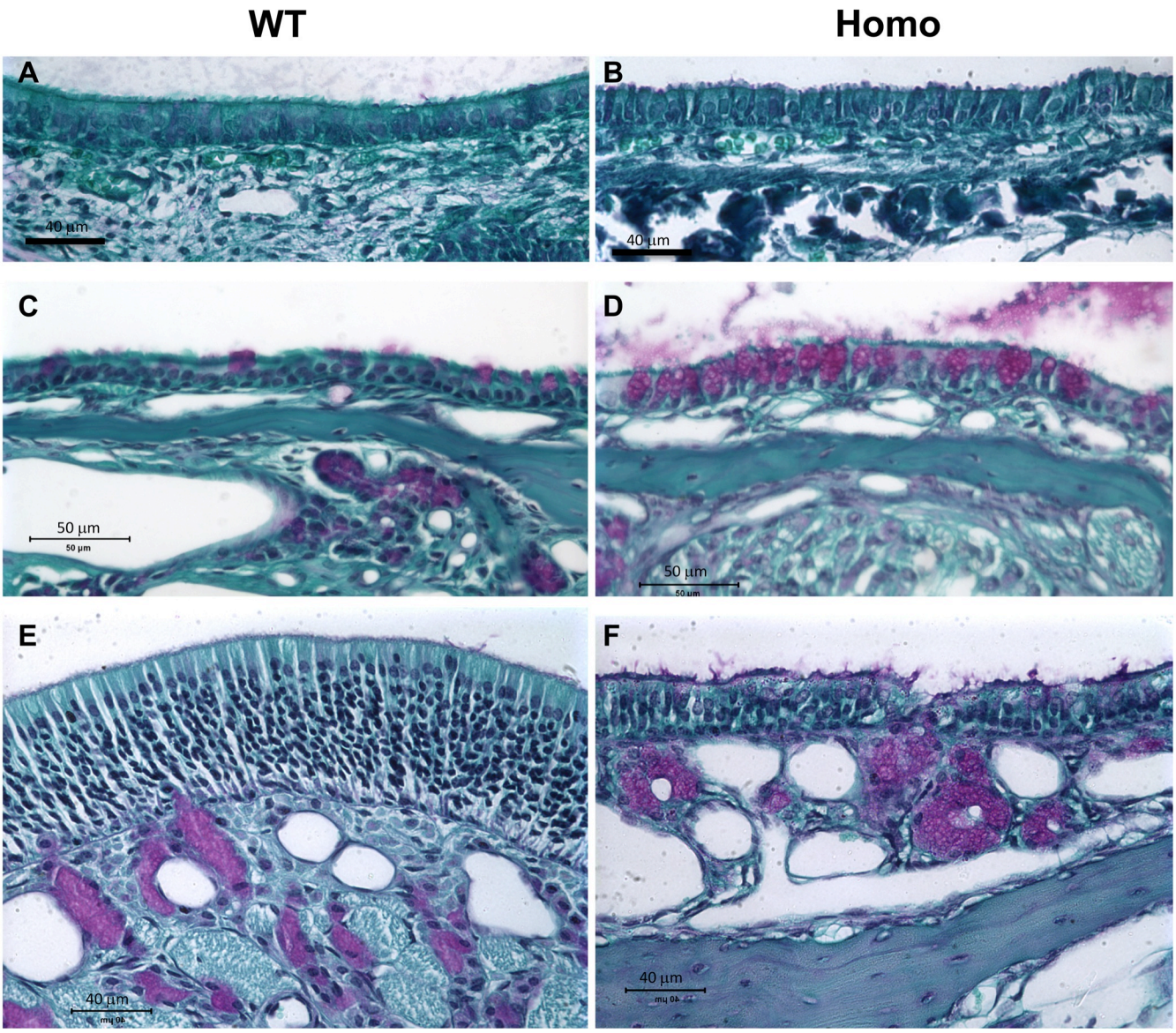

SI Figure S10. Periodic Acid Schiff's (PAS) staining for glycoproteins in mucus (pink/purple). (**A**) WT section of P1 septal respiratory epithelium compared to (**B**) the septum respiratory epithelium from a *Camsap3*$^{tm1a/tm1a}$. Scale bars, 40 µm. (**C**) P204 WT respiratory epithelium compared to (**D**) P204 *Camsap3*$^{tm1a/tm1a}$, which showed goblet cell hyperplasia. Scale bars, 50 µm. (**E**) P204 WT nasal olfactory epithlium compared to (**F**) P204 *Camsap3*$^{tm1a/tm1a}$. Scale bars, 40 µm.

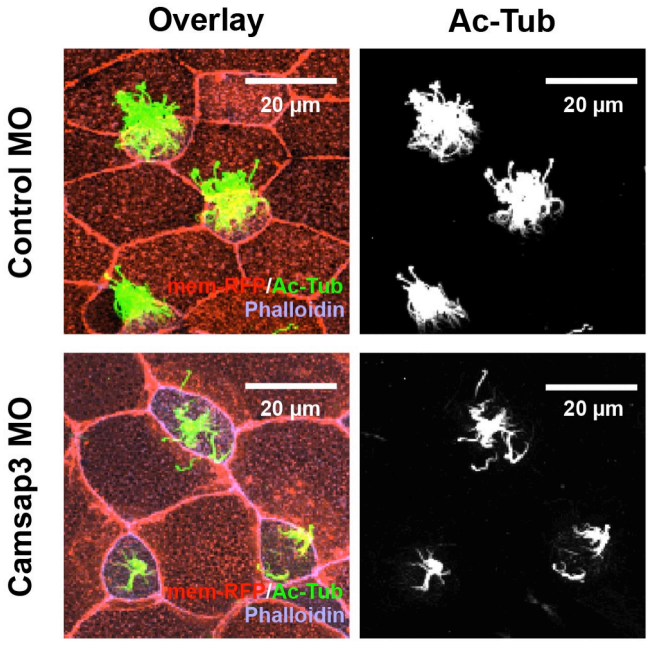

SI Figure S11. Reduction of CAMSAP3 in MCCs of Xenopus embryos affects the morphology of cilia on MCCs. Xenopus embryo injected with control and Camsap3-MOs were stained with anti-acetylated-tubulin (Ac-Tub, green) for cilia, and with phalloidin-cy7 (Phalloidin, violet) for actin (marks cell boundary). Membrane-RFP marker was also co-injected with control or Camsap3-MOs and serves as injection control (mem-RFP, red). Control-MO-injected embryos exhibited robust cilia on MCCs (top), while Camsap3-MO-injected embryos tend to have MCCs with shorter and/or sparse cilia (bottom). Representative images from seven independent experiments are shown. Scale bars, 20 μm.

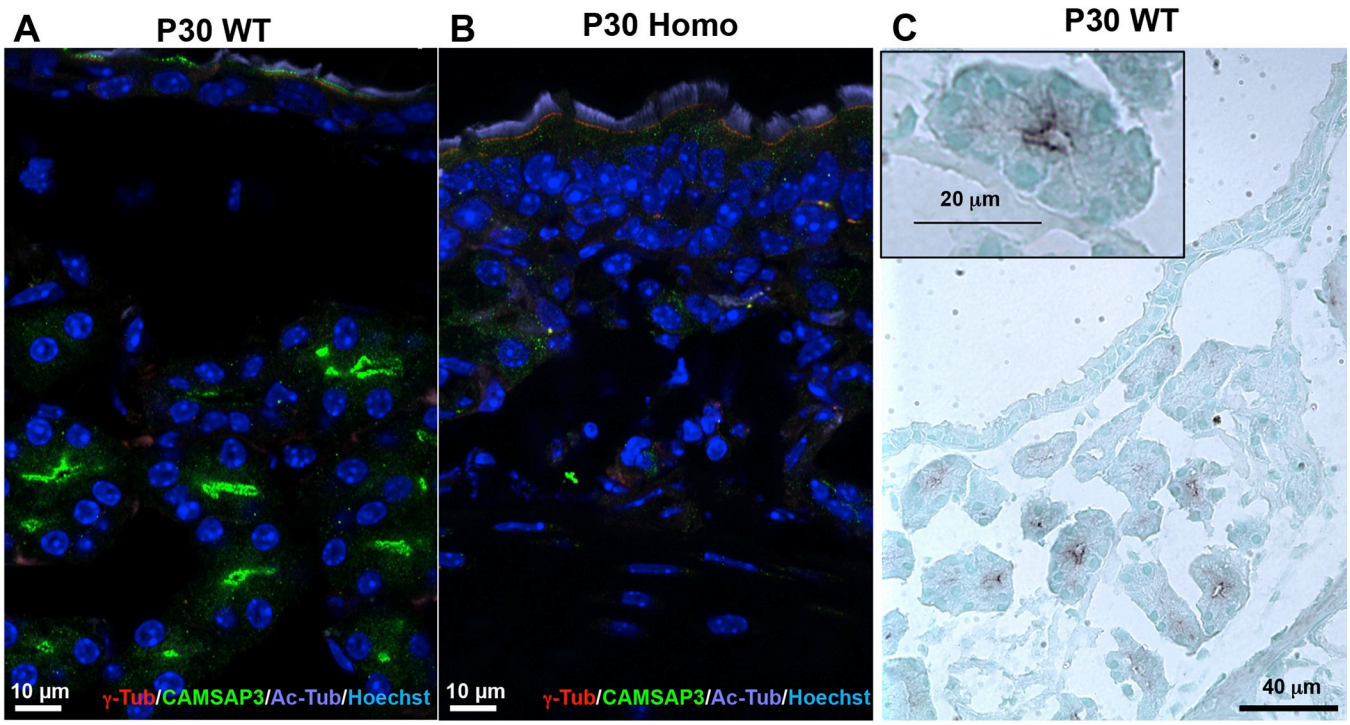

SI Figure S12. CAMSAP3 is located at the apical surface of respiratory epithelia and the epithelial cells of submucosal glands. Immunofluorescent images of septum epithelia from WT (**A**) and *Camsap3*$^{tm1a/tm1a}$ (**B**) at age of P30. Anti-CAMSAP3-M (Green), anti-γ-tubulin (Red), anti-acetylated-α-tubulin (Violet), and Hoechst 33342 (Blue, nuclei). Scale bars, 10 μm. **C.** CAMSAP3 signals (anti-CAMSAP3-M antibody, brown NovaRED stain) are mostly located at the apical cortex of epithelial cells in the acini of submucosal glands in young adult WT. The inset shows an enlarged image of a submucosal gland. Similar expression patterns are found in small intestinal epithelial cells (15), suggesting that CAMSAP3 may be involved in organizing MT polarity.

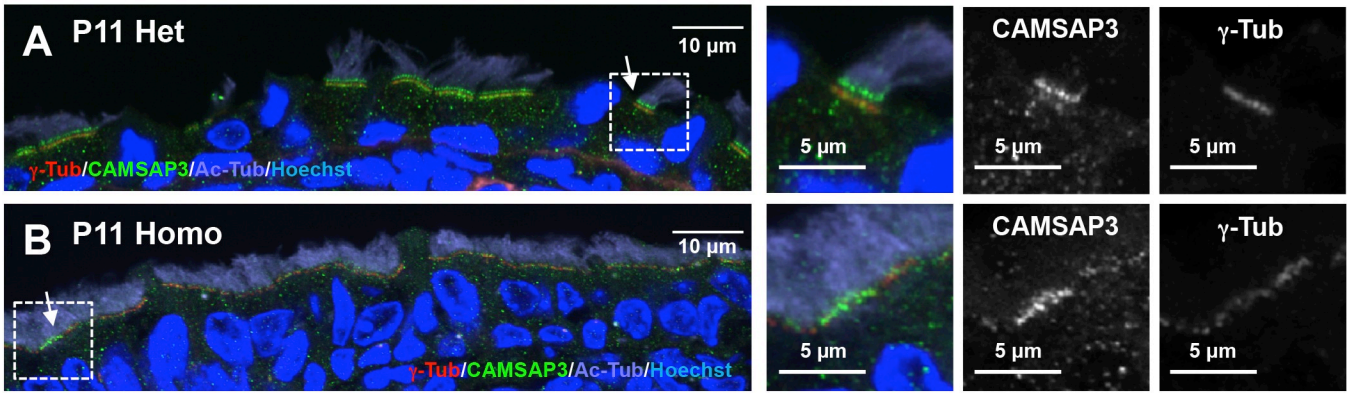

SI Figure S13. CAMSAP3 distribution in MCCs. Immunofluorescent images of nasal MCCs on turbinates from *Camsap3*$^{tm1a/+}$ (**A**) and *Camsap3*$^{tm1a/tm1a}$ (**B**) mice at P11. Labeling in the *Camsap3*$^{tm1a/+}$ shows two CAMSAP3 lines or simply the upper green line (arrow in **A**). Most MCCs from the *Camsap3*$^{tm1a/tm1a}$ have no CAMSAP3 staining or, if present, it is associated with only the lower green line, i.e., with the basal bodies (arrow in **B**). Merged and individual channels of the boxed regions in the left panels are shown on the right. Anti-CAMSAP3-M (CAMSAP3, Green), anti-γ-Tubulin (γ-Tub, Red), anti-acetylated-α-Tubulin (Ac-Tub, Violet), and Hoechst 33342 (Blue, nuclei). Scale bars as indicated.

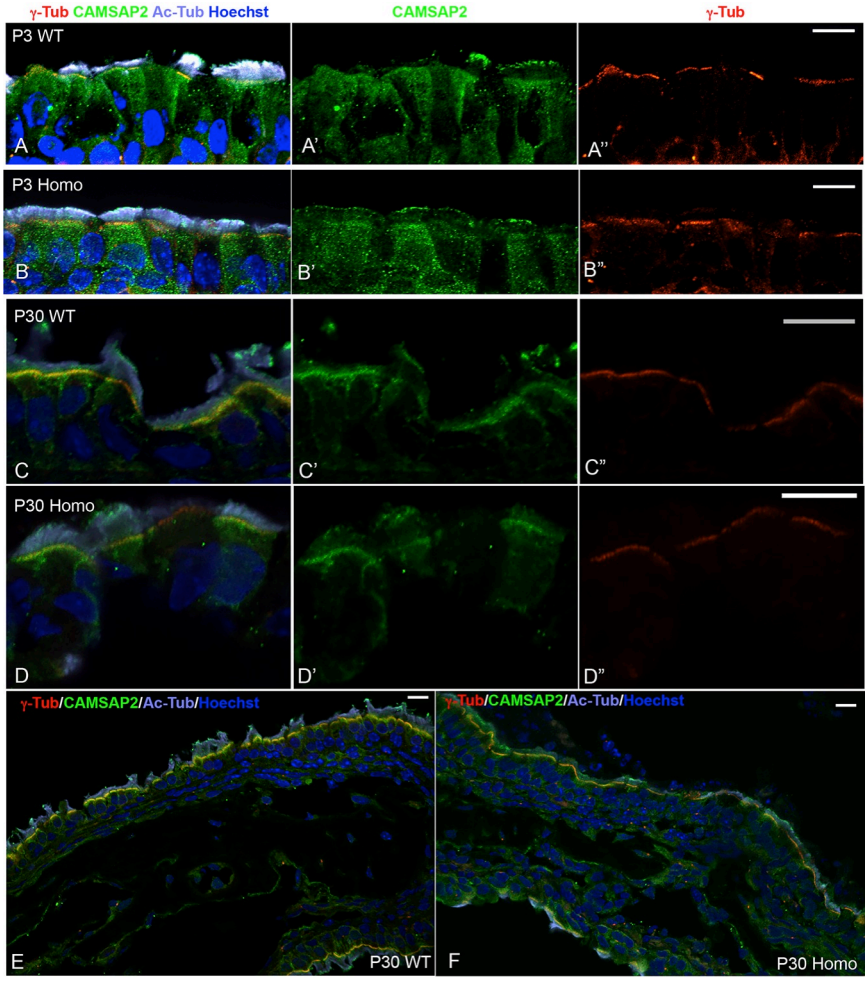

SI Figure S14. CAMSAP2 expression patterns in MCCs are different from CAMSAP3. Immunofluorescent images of nasal MCCs from WT (**A, C, E**) and *Camsap3*$^{tm1a/tm1a}$ (**B, D, F**) at P3 (**A-B**) and P30 (**C-F**). There are no differences in CAMSAP2 staining patterns between WT and *Camsap3*$^{tm1a/tm1a}$ littermates at both P3 and P30. Antibodies include: anti-CAMSAP2 (Green), anti-γ-Tubulin (γ-Tub, Red), anti-acetylated-α-Tubulin (Ac-Tub, Violet), and Hoechst 33342 (Blue, nuclei). Scale Bars: 10 μm. (**A-B**) MCCs from P3 WT (**A**) and *Camsap3*$^{tm1a/tm1a}$ littermates (**B**). CAMSAP2 (green **A'**, **B'**) staining is found throughout the cytoplasm of MCCs. In contrast to the two lines of CAMSAP3-staining (**Fig. 5C-C'**), no obvious CAMSAP2-green lines are found near basal bodies (γ-Tub, red line). (**C-D**) MCCs from P30: WT (**C**) and *Camsap3*$^{tm1a/tm1a}$ littermates (**D**). CAMSAP2 staining (green, **C'**, **D'**) co-localizes with basal bodies (γ-Tub, red line **C"**, **D"**), while CAMSAP3 staining is observed above the basal bodies (**Fig. 5E-E', G**). (**E-F**) MCCs are imaged at lower magnification at P30, showing co-localization of CAMSAP2 staining (green) with the basal body marker (γ-Tub, red).

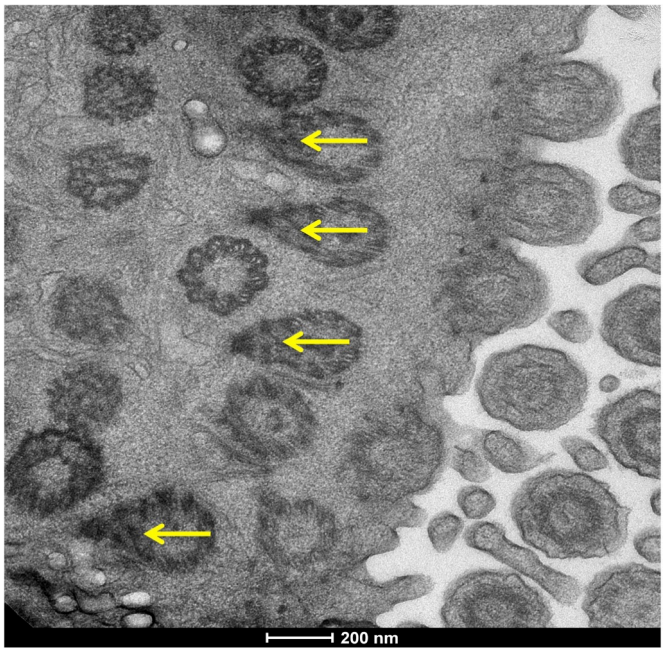

SI Figure 15. A representative TEM image showing basal feet in a WT-MCC in the nasal cavity (P30). Yellow arrows indicate basal feet with aligned orientations. Scale bar, 200 nm.

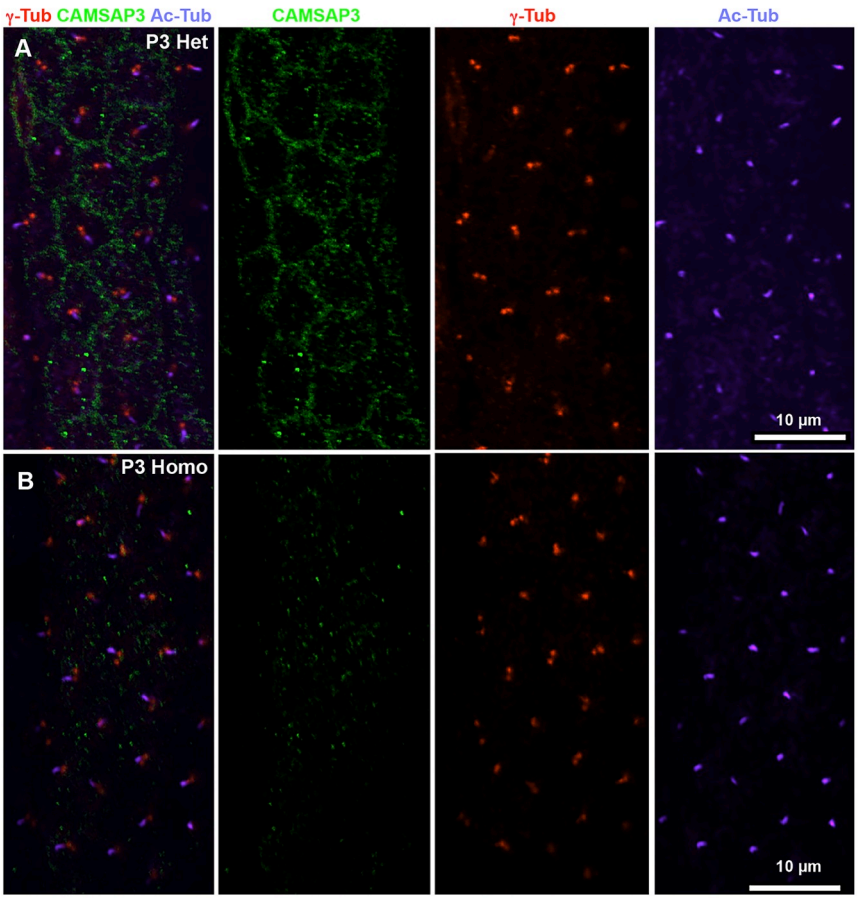

SI Figure 16. The primary cilia of cochlear epithelial cells of *Camsap3*$^{tm1a/tm1a}$ appear normal. Immunofluorescent images of cochlear epithelial cells within the organ of Corti of WT (**A**) and *Camsap3*$^{tm1a/tm1a}$ (**B**) at P3 are shown. Antibodies: anti-CAMSAP3-M (Green), anti-γ-Tubulin (γ-Tub, red, the basal body marker), anti-acetylated-α-Tubulin (Ac-Tub, violet, the cilium marker), and Hoechst 33342 (Blue, nuclei). Scale Bars: 10 μm. The epithelial cells of *Camsap3*$^{tm1a/tm1a}$ (**B**), with minimal CAMSAP3 signals, have normal primary cilia (violet) and basal bodies (red), and their staining patterns are similar to those of WT. CAMSAP3 signals (**A**) seldom co-localize with basal body signals, but are found around the cellular boundary at the apical cortex, similar to a previous report (15)

Movies and Audio

Movie S1: Audio recordings of 5 *Camsap3*$^{tm1a/tm1a}$ mice. *Camsap3*$^{tm1a/tm1a}$ mice make wheezing sounds, as shown in *SI Appendix* Fig. S4. Pay attention to sound.

Movie S2. Live imaging of multiciliary synchronized motion and directional flow (moving particles) on the surface of MCCs from a WT nasal cavity. Related to Fig. 4A.

Movie S3. Live imaging of multiciliary beating on the surface of MCCs from the nasal cavity of a *Camsap3*$^{tm1a/tm1a}$. Reduced directional flow is observed. Related to Fig. 4A.

Movie S4. Live imaging of multiciliary synchronized motion and directional flow (moving particles) on the surface of MCCs from a WT tympanic cavity. Related to Fig. 4A.

Movie S5. Live imaging of multiciliary beating on the surface of MCCs from the tympanic cavity of a *Camsap3*$^{tm1a/tm1a}$, showing no motion or slow rotational motion. Related to Fig. 4A

Movie S6. Live imaging of multiciliary synchronized motion and directional flow (moving particles) on the surface of MCCs from a WT trachea. Related to Fig. 4A.

Movie S7. Live imaging of multiciliary beating on the surface of MCCs from the trachea of a *Camsap3*$^{tm1a/tm1a}$, showing no motion or slow rotational motion. Related to Fig. 4A.

Movie S8. Live imaging of directional flow tracked by fluorescent-beads moving across the surface of MCCs from a Xenopus embryo injected with control-MO. Related to Fig. 4B.

Movie S9. Live imaging of fluorescent beads drifting on the surface of MCCs from a Xenopus embryo injected with Camsap3-MO. Related to Fig. 4B.

Audio S1. Wheezing sounds produced by a *Camsap3*$^{tm1a/tm1a}$. The original sampling rate does not allow humans to perceive the high-frequency components (>20 kHz). However, when the same sound track was played at a fifth of the original sampling rate, the high frequency components become audible to human ear.

References

1. Werner ME & Mitchell BJ (2013) Using Xenopus skin to study cilia development and function. *Methods in enzymology* 525:191-217.
2. Sive HL, R.M. Grainger, and R.M. Harland ed (1998) *The Early Development of Xenopus laevis: A Laboratory Manual* (Cold Spring Harbor Laboratories, Plainview, New York).
3. Rasband, W.S., ImageJ, U.S. National Institutes of Health, Bethesda, Maryland, USA, https://imagej.nih.gov/ij/, 1997-2018.
4. Smith CM*, et al.* (2012) ciliaFA: a research tool for automated, high-throughput measurement of ciliary beat frequency using freely available software. *Cilia* 1:14.
5. PAS electronic reference: www.ihcworld.com/_protocols/special_stains/pas.htm.
6. H&E electronic reference: www.ihcworld.com/_protocols/special_stains/HE_Harris.htm.
7. Takahashi S*, et al.* (2016) Cadherin 23-C Regulates Microtubule Networks by Modifying CAMSAP3's Function. *Scientific reports* 6:28706.
8. Zheng J*, et al.* (2000) Prestin is the motor protein of cochlear outer hair cells. *Nature* 405(6783):149-155.
9. Zheng J*, et al.* (2013) Marshalin, a microtubule minus-end binding protein, regulates cytoskeletal structure in the organ of Corti. *Biol Open* 2(11):1192-1202.
10. Jiang K*, et al.* (2014) Microtubule minus-end stabilization by polymerization-driven CAMSAP deposition. *Developmental cell* 28(3):295-309.
11. Sengupta S*, et al.* (2010) Interaction between the motor protein prestin and the transporter protein VAPA. *Biochimica Et Biophysica Acta-Molecular Cell Research* 1803(7):796-804.
12. Kim SK*, et al.* (2018) CLAMP/Spef1 regulates planar cell polarity signaling and asymmetric microtubule accumulation in the Xenopus ciliated epithelia. *The Journal of cell biology* 217(5):1633-1641.
13. Uhlen M*, et al.* (2015) Proteomics. Tissue-based map of the human proteome. *Science* 347(6220):1260419.
14. Yau KW*, et al.* (2014) Microtubule minus-end binding protein CAMSAP2 controls axon specification and dendrite development. *Neuron* 82(5):1058-1073.
15. Toya M*, et al.* (2016) CAMSAP3 orients the apical-to-basal polarity of microtubule arrays in epithelial cells. *Proceedings of the National Academy of Sciences of the United States of America* 113(2):332-337.